INTERNATIONAL JOURNAL OF HYDROGEN ENERGY 42 (2017) 28898–28909

Available online at www.sciencedirect.com

ScienceDirect

journal homepage: www.elsevier.com/locate/he

A novel approach for dynamic gas conditioning for PEMFC stack testing

János Kancsár [a,*], *Michael Striednig* [b], *David Aldrian* [b], *Alexander Trattner* [b], *Manfred Klell* [b,c], *Christoph Kügele* [d], *Stefan Jakubek* [e]

[a] *Christian Doppler Laboratory for Innovative Control and Monitoring of Automotive Powertrain Systems, TU Wien, Getreidemarkt 9/325-A5, 1060 Vienna, Austria*

[b] *HyCentA Research GmbH, Inffeldgasse 15, 8010 Graz, Austria*

[c] *Graz University of Technology, Institute for Internal Combustion Engines and Thermodynamics, Inffeldgasse 19, 8010 Graz, Austria*

[d] *AVL List GmbH, Hans List Platz 1, 8020 Graz, Austria*

[e] *TU Wien, Institute of Mechanics and Mechatronics, Division of Control and Process Automation, Getreidemarkt 9/325-A5, 1060 Vienna, Austria*

ARTICLE INFO

Article history:
Received 7 June 2017
Received in revised form
8 September 2017
Accepted 11 September 2017

Keywords:
PEMFC testbed
PEMFC stack testing
Nonlinear multivariate control
Differential flatness
Exact linearisation
Nonlinear dynamic modelling

ABSTRACT

The air supply to the polymer electrolyte membrane fuel cell (PEMFC) stack is crucial for the performance of a PEMFC system. To enable modular and transient testing of the stack during development, a novel dynamic gas conditioning system is presented. To meet the requirements of transient stack testing, different hardware concepts for the testbed are evaluated and an experimental setup is realised. The thermodynamic states of this system are coupled through various relations and represent a nonlinear multivariate control problem. For controller design a dynamic nonlinear model of the system is derived and parameterised with measurements from the testbed. To decouple the system and achieve a good transient response the model-based nonlinear control concept of exact input-output linearisation is applied. Based on the decoupled system, a Two-Degree-of-Freedom (2DoF) controller is designed. The application of this nonlinear control concept on the realised hardware setup shows that accurate trajectory tracking during dynamic set point changes is ensured. Experimental results are presented to validate the control performance.

Introduction

The limitation of global warming to less than 2 °C represents the greatest challenge of our era [1]. In order to meet 21st Conference of the Parties (COP21) objectives, a clear transition from carbon-based energy sources towards renewables is mandatory. Hydrogen as a green energy carrier complementing electricity will play the key role for this transition

* *Corresponding author.*
E-mail address: janos.kancsar@tuwien.ac.at (J. Kancsár).
https://doi.org/10.1016/j.ijhydene.2017.09.076

in all sectors (mobility and transport, industry, agriculture and households) [2].

Global transport is estimated to double between now and 2050 under a business-as-usual scenario whereas, automotive emission regulations are getting more stringent [3]. Electrification and hybridisation are essential technologies to meet these challenges [4]. Hydrogen powered fuel cell electric vehicles (FCEVs) [5–7] are a promising alternative to conventional powertrains, since polymer electrolyte membrane fuel cells (PEMFC) allow an energy-efficient, resource-efficient and emission-free conversion of regenerative produced hydrogen and offer the potential to achieve low costs in mass production. However, several key issues regarding degradation, cold-start performance, efficiency, dynamic response and costs have to be solved to achieve an increasing market penetration [8].

To obtain a high power output, single fuel cells are combined to fuel cell stacks. In order to operate the stack properly, pressure, temperature, mass flow and humidity of reaction gases have to be controlled by balance of plant (BoP) components, e.g. humidifier, blower, anode recirculation etc. within tight limits. This combination of stack and BoP components is often referred to as a fuel cell system. PEM fuel cell systems are complex and highly integrated mechatronic systems.

Automotive applications of fuel cells are challenging due to variable operating conditions, load cycles, start-up and shut-down cycles, humidity cycles, freeze-thaw cycles and air contamination. Moreover, automotive fuel cell systems are operated dynamically, which means that the set points are changed continuously during operation. In order to successfully integrate the fuel cell system into the electric power train and to prevent degradation and thus prolong lifetime, it is important to understand the transient behaviour of the fuel cell stack. In addition, current development processes are cost and time intensive due to missing cross-links between stack and BoP-component development. In consequence, the risk of unexpected interactions and necessary modifications increases significantly and potentials regarding durability, efficiency and performance remain unused.

At present, turnkey solutions for modular test infrastructure are hardly available. Most systems are proprietary in-house solutions of automotive manufacturers or research institutes, since hardware design and the development of appropriate control strategies, in particular, are challenging.

First and foremost, the understanding of dynamic characteristics of fuel cells is important to efficiently design, operate and optimise the fuel cell system as well as specialised test infrastructure [9]. Hence, the dynamic behaviour of fuel cells has been the focus of many studies. In the presented literature various tests regarding dynamic behaviour of fuel cells were performed.

Wang et al. [10,11] presented dynamic three-dimensional fuel cell models and estimated time constants for different transient phenomena such as electrochemical double-layer discharging, gas transport through gas diffusion layer (GDL) and membrane hydration. Their results show that the time to reach steady-state operation after a step change is in the order of ten seconds. Kang et al. [12,13] developed a membrane humidifier model. They investigated the influences of inflowing air and humidity during load changes on the performance of PEMFCs. Their results show that the model can be used to optimise the inlet air humidity.

Although simulations give a good insight into phenomena, which are not measurable, novel control strategies require experimental validations on physical fuel cell stacks which is challenging [14] and therefore rare in literature.

Migliardini et al. [15] investigated how different humidification methods affect the performance of a fuel cell stack. They performed steady state measurements with internal and external humidification. Their data show that the change of humidity takes about 2–3 min to reach steady state. In Refs. [16–18] the authors investigated the start-up behaviour of fuel cells. They stress the importance of understanding transient phenomena for the optimisation of design and operational strategy. Zhang et al. [19] studied the effects of back pressure, relative humidity and air stoichiometry variations on the overall performance. Although they investigated different set points, they neglected the transients during set point change. Santarelli et al. [20,21] analysed the effect of different operating variables on the polarisation curve. Transition between set points was neglected and steady-state performance was evaluated. They used a ramp to change the set point, waited until steady state was reached and then performed their measurements. Corbo et al. [22] used dynamic driving cycles to analyse the effect of dynamic conditions on a fuel cell. Based on measurements they deduced a management strategy for automotive PEMFC systems. Their experimental analyses show that excursions outside the optimal working region are acceptable if they last for times comparable to those of fast acceleration phases (10 s as order of magnitude).

In additional studies tests regarding dynamic behaviour of PEMFCs were performed [23–28]. However, due to specific hardware setups some input variables (e.g. humidity) could only be varied slowly and tests were performed with constant values of this variable. The transient control of testbeds is complex and requires sophisticated control methods such as nonlinear multivariate control. Kancsár et al. [29] studied the concept of flatness-based feedforward control to operate a dynamic fuel cell testing environment. Such concepts are also implemented as control strategies in fuel cell systems. Danzer et al. [30,31] applied a flatness-based control concept for the regulation of oxygen excess ratio and cathode pressure, and Hähnel et al. [32] applied nonlinear model predictive control to deal with nonlinear characteristics of the fuel cell. Fang et al. [33] studied the temperature regulation of a fuel cell test bench. They designed a sliding-mode-based coolant regulation, which accounts for occurring time delay and heat generated by the fuel cell stack.

In this paper the issue of transient stack testing is addressed and a novel concept (hardware and control strategy) for dynamic gas conditioning is provided. Different possible hardware concepts, which are suitable for transient testing, are evaluated. Based on the evaluation a test setup is constructed and a nonlinear multivariate model is derived, which describes the coupling of the thermodynamic quantities in the system. To yield a valid system description a method for proper model parameterisation with measurements performed on the testbed is given. Based on the dynamic model a nonlinear multivariate control concept, which deals with the coupling of the thermodynamic quantities, is

applied. Finally, the control performance is evaluated experimentally on the testbed.

This paper is structured as follows: General requirements of fuel cell stack testbeds are discussed in Section "Requirements for transient stack testing", different hardware concepts are evaluated in Section "Hardware concept" and an experimental test setup is assembled. The coupling of thermodynamic quantities is discussed and a dynamic multivariate model of the testbed is derived in Section "Nonlinear multivariate control of testbed" and parameterised with measurements. Based on the dynamic model a nonlinear multivariate control concept is applied, which deals with the coupling of the thermodynamic quantities. Finally, the control performance is evaluated with measurements in Section "Results and Measurements" and conclusions are given in Section "Conclusion".

Requirements for transient stack testing

In the following, requirements of fuel cell stack testbeds regarding reactant gas conditioning are discussed and the main challenges are highlighted. The focus of this paper lies on cathode air conditioning; however, the presented concepts can also be adapted for the anode.

The dynamic operation of fuel cells under automotive boundary conditions requires set point changes and response times faster than 700 ms. Consequently, the gas conditioning system at stack testbeds must provide the adequate amount of reaction gases at specific pressure, temperature and humidity instantaneously, since these thermodynamic quantities determine the performance and degradation of the fuel cell stack.

First, a sufficient supply of reactants has to be provided in order to avoid reactant shortage (hydrogen and oxygen starvation) during operation, which reduces the lifetime of the fuel cell significantly [34,35]. Second, the reactant gas pressure must be controlled within tight limits and depending on the operation point [36], since the power output of the stack is affected. Moreover, the system pressure regulation is crucial for the lifetime of the fuel cell stack, since a significant pressure difference between anode and cathode as well as pressure pulses can damage the membrane [37]. Third, the humidity of the inflowing gas has to be controlled to avoid dry-out or swelling of the membrane, which causes degradation and thus reduction of the lifetime of the fuel cell [38]. Finally, the temperature of the reactants has to be controlled in the range of 60 °C.

In order to achieve a fast response of the gas conditioning system, the hardware components for heating and cooling, humidification as well as for pressure and flow regulation have to be designed specifically. From the aspect of control theory the challenge is twofold. First, the physical processes, governing the dynamics of the testbed, have to be modelled and parameterised with measurements from the testbed. Second, the thermodynamic quantities (pressure, temperature, humidity and massflow) are physically coupled by various relations, and thus changing one quantity affects the others. These circumstances yield a coupled nonlinear multivariate system, which has to be decoupled and the desired output quantities have to be controlled in a way that good trajectory tracking and disturbance rejection are ensured.

Hardware concept

In order to meet the discussed requirements and constraints of fuel cell stack testbeds, the hardware concept of the conditioning system is designed to enable the independent adjustment of the thermodynamic quantities pressure, temperature, humidity and massflow. Therefore, the system is divided into the following four functional blocks: flow control, thermal management, humidification and back pressure control, see Fig. 1.

Fig. 1 – Schematic of functional blocks.

This chapter gives an overview on different possible solutions for each function and presents a comparative evaluation and the actual hardware implementation.

Flow control

The following three concepts for mass flow control have been investigated with special regards to the requirements of the actual application (see Fig. 2).

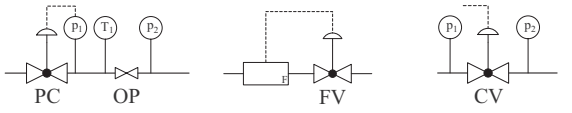

(a) Concept A_F (b) Concept B_F (c) Concept C_F

Fig. 2 – Flow control concepts.

In concept A_F (Fig. 2a) the mass flow is regulated by an orifice plate (OP) and can be described as a function of pressure ratio $\Pi = p_2/p_1$, inlet temperature T_1, cross-sectional area A of the orifice plate and thermo-physical properties of the medium (isentropic exponent κ, specific gas constant R). Consequently, the mass flow is controlled by varying the inlet pressure p_1 by a remote actuated pressure regulator (PC). The descriptive nonlinear flow equation for an isentropic change of state is shown below [39].

$$\dot{m} = A p_1 \sqrt{\frac{2}{RT_1}}\psi, \qquad \psi = \sqrt{\frac{\kappa}{\kappa-1}\left(\Pi^{\frac{2}{\kappa}} - \Pi^{\frac{\kappa+1}{\kappa}}\right)}, \quad \Pi = \frac{p_2}{p_1}. \tag{1}$$

The function ψ has its maximum value at the so-called critical pressure ratio, which is given by

$$\Pi_{\text{crit.}} = \left(\frac{p_2}{p_1}\right)_{\text{crit.}} = \left(\frac{2}{\kappa+1}\right)^{\frac{\kappa}{\kappa-1}}. \tag{2}$$

From this, $\psi_{\max}$ for the critical flow derives as

$$\psi_{max} = \left(\frac{2}{\kappa+1}\right)^{\frac{1}{\kappa-1}} \sqrt{\frac{\kappa}{\kappa+1}}. \quad (3)$$

Above the critical pressure ratio $\Pi_{crit.}$ the massflow given by Eq. (1) becomes independent of the downstream pressure p_2 and is linearly dependent on p_1. This physical property is utilised by concept A_F. In concept B_F (Fig. 2b) the mass flow is set by a flow controller, consisting of a flow measuring transducer (F) (e.g. coriolis flow meter) and an actuator (FV) (e.g. proportional valve). In concept C_F (Fig. 2c) the mass flow is controlled by changing the opening profile and respectively the flow coefficient of a proportional valve (CV).

In comparison to concept A_F, concept B_F shows poor response time as well as unstable and imprecise measurements as consequence of the slower mass flow measurement. Furthermore, results of various tests pointed out that the regulation of the mass flow via the inlet pressure in concept A_F instead of the opening profile of a regulating valve in concept C_F is more expedient due to the occurring pressure ratio. The mass flow $\dot{m}$ set with concept A_F is linearly dependent on the inlet pressure in a large range of the characteristic diagram, which facilitates the control and therefore is preferred over the others.

Heating

The two main concepts A_H and B_H for thermal management of a gas flow are shown in Fig. 3a and b. In concept A_H the required temperature is set by dynamic heating (heat exchanger (HEX)), respectively cooling of a single gas stream. In concept B_H the required temperature is provided by mixing of two streams with different temperature in a specific ratio to reach a predefined temperature. In Fig. 3a (concept A_H) the target temperature T_2 depends on the inlet temperature T_1, the mass flow $\dot{m}$ and the thermal power flow $\dot{Q}_{in}$.

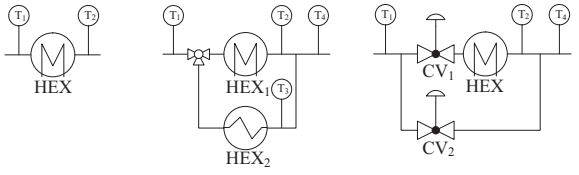

(a) Concept A_H (b) Concept B_H (c) Concept C_H

Fig. 3 – Thermal management concepts.

Especially the thermal inertia of the heat exchanger and the dependence of the mass flow temperature T_2 on the mass flow itself involve great challenges regarding the dynamics of the heat exchanger. This relation is given by Eq. (4) for ideal gases.

$$T_2 = \frac{\frac{\dot{Q}_{in}}{\dot{m}} + c_{p,1}T_1}{c_{p,2}}. \quad (4)$$

In contrast, the intended gas temperature T_4 in Fig. 3b (concept B_H) is largely unaffected by the total mass flow $\dot{m}$ as long as the heat exchangers provide enough power to keep the temperatures T_2 and T_3 constant. In this concept the temperature depends on the valve position $\zeta = \dot{m}_2/\dot{m}_3$ that defines the mass flow ratio of both streams. The corresponding equation is given by

$$T_4 = \frac{\zeta c_{p,2}T_2 + c_{p,3}T_3}{(\zeta+1)c_{p,4}}, \quad \zeta = \frac{\dot{m}_2}{\dot{m}_3}. \quad (5)$$

Both concepts were field-tested in the course of the testbed development. Results pointed out that concept B_H allows a faster adjustment of the temperature. The reason for that is not only the quick variation of the mass flow ratio ζ, but also the possibility to vary the temperature T_2 of the warmer stream up to a level of 200 °C. Subsequently, concept B_H is chosen and further developed for the specific requirements.

The wide mass flow range requires a certain valve size to limit the pressure loss at high flow rates. Consequently, the control range is reduced at low mass flows and the temperature can be controlled only with little precision. Field tests with a three-port valve confirm this trade-off, and thus it has been replaced with two control valves (CV_1) and (CV_2). Furthermore, on the basis of the required temperature range of 40–80 °C, it is not necessary to build in the heat exchanger (HEX_2) in the colder gas path (ambient temperature below 40 °C at all times) although it would increase the dynamics. The final concept for temperature regulation is shown in Fig. 3c (concept C_H).

Humidification

Various humidification methods like saturated steam injection, liquid water injection and ultrasonic humidifiers are industrial standard in different applications. They have been evaluated theoretically with regard to the existing technical and economic boundary conditions and subsequently, only the saturated steam injection was further considered. This method provides the necessary steam mass flow and pressure, while at the same time having a low technical effort and lower costs compared to other methods. Furthermore, it allows a highly dynamic and precise injection of steam and it minimises, at the same time, the risk of unintended droplets in the humid air.

The applied humidification method is shown in Fig. 4 and consists of an electrical pump P that feeds liquid water into the steam boiler (D_1). Subsequently, a heat exchanger (HEX) superheats the steam up to a temperature level of 160 °C. Finally, the amount of steam fed to the air is controlled via a sliding gate control valve (CV). All pipes and valves are insulated and heated.

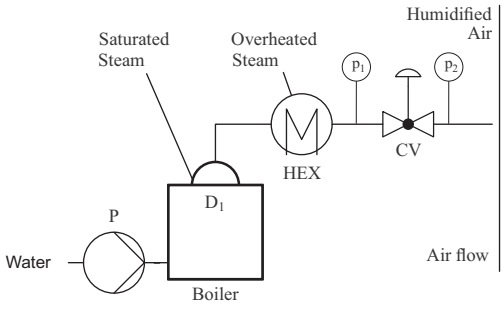

Fig. 4 – Humidification by steam boiler.

This concept has the advantage, that it can easily be scaled to the application and that the pressure in the steam boiler can be chosen such that a critical pressure ratio is ensured for steam injection, which facilitates control.

Back pressure control

The stack pressure is controlled in a range from 1.1 to 3 bar(a). Two concepts, shown in Fig. 5, have been evaluated theoretically. First, the pressure p_1 is adjusted by a back pressure regulator (BPC) (Fig. 5a, concept A_P) and second, a sliding gate control valve (CV) is used (Fig. 5b, concept B_P). Two requirements are essential for the control of the back pressure. First, the back pressure valve should not introduce additional dynamics through an underlying control loop. Second, the back pressure valve should be able to be actuated independently of the system pressure. Concept B_P fulfils both requirements, therefore it was chosen.

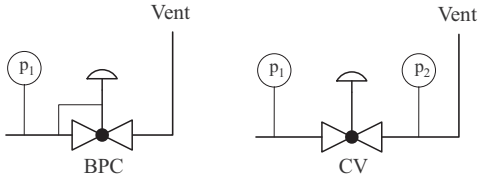

Fig. 5 – Back pressure control concepts.

Fuel cell stack

An applied measuring section represents the fuel cell stack as part of the hardware construction. It includes sensors for pressure p, air temperature T, humidity φ and mass flow $\dot{m}$. A real fuel cell stack would act as an additional pressure resistance, which is in series with the back pressure valve.

Nonlinear multivariate control of testbed

In the following, a model is derived from the hardware concept introduced in Section "Hardware concept". Based on this model a nonlinear control concept [29] is introduced, which deals with the coupling of the nonlinear multivariate system. Further, the implementation of this nonlinear multivariate control concept to the fuel cell stack testbed is shown (Fig. 6).

Dynamic model of hardware setup

A schematic of the hardware setup introduced in Section "Hardware concept" is shown in Fig. 6. The hardware components described in Section "Hardware concept" are represented by the blocks *Gas* (Concept A_F, Fig. 2a), *Heater* (Concept C_H, Fig. 3c) and *Steam* (Fig. 4). From this, the system dynamics can be derived. The gas mass in the system is defined by

$$m = m_G + m_S, \tag{6}$$

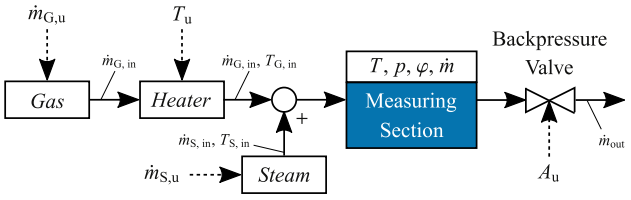

Fig. 6 – Gas conditioning system model applied for nonlinear control.

where m_G represents the gas mass and m_S the steam mass. The mass balance equations of the gas components are given by

$$\begin{aligned} \frac{d}{dt}m_G &= \dot{m}_{G,\,in} - \dot{m}_{G,\,out}, \\ \frac{d}{dt}m_S &= \dot{m}_{S,\,in} - \dot{m}_{S,\,out}, \end{aligned} \tag{7}$$

where the first terms represent the inflowing gas streams, and the second terms represent the outflowing mass streams. The outflowing gas streams are given by the mass fraction of the total outflowing mass stream:

$$\dot{m}_{G,\,out} = \frac{m_G}{m}\dot{m}_{out}, \quad \dot{m}_{S,\,out} = \frac{m_S}{m}\dot{m}_{out}, \tag{8}$$

where $\dot{m}_{out}$ is given by Eq. (1). The temperature dynamics can be derived from the energy balance of the system [29]. To account for the thermal inertia of the system, the additional factors γ_G to the gas component and γ_S to the steam components are introduced. The thermal inertia of the system arises mainly from the hardware realisation of the testbed (e.g. piping material and cross sections/volume), which affects the system dynamics. The resulting equation yields

$$\begin{aligned} \frac{d}{dt}T = \frac{1}{m_G c_{v,G} + m_S c_{v,S}} \cdot \Big(& \gamma_G \dot{m}_{G,\,in} c_{p,G} T_{G,\,in} + \gamma_S \dot{m}_{S,\,in}\left(c_{p,S}T_{S,\,in} \right. \\ & \left. + r_0\right) - \frac{1}{m}\dot{m}_{out}\left(\gamma_G m_G c_{p,G} T + \gamma_S m_S \left(c_{p,S}T + r_0\right)\right) \\ & - \gamma_G \frac{d}{dt} m_G c_{v,G} T - \gamma_S \frac{d}{dt} m_S (c_{v,S}T + r_0)\Big), \end{aligned} \tag{9}$$

where T is the temperature in the system, $c_{v,G}$ and $c_{v,S}$ are the heat capacities at constant volume, $c_{p,G}$ and $c_{p,S}$ are the heat capacities at constant pressure, $T_{G,\,in}$ is the temperature of the inflowing gas mass stream, $T_{S,\,in}$ is the temperature of the inflowing steam mass stream and r_0 is the latent heat of steam.

The system pressure p can be determined by using the ideal gas law

$$pV = (m_G R_G + m_S R_S)T, \tag{10}$$

where V represents the volume and R_G and R_S are the gas constants. Here it is to be noted that the volume includes all piping in the hardware setup. Therefore, by reducing the piping volume, the dynamics of the system will change.

The relative humidity in the system is given by

$$\varphi = \frac{X}{\frac{R_G}{R_S} + X} \cdot \frac{p}{p_W^s(T)}, \quad X = \frac{m_S}{m_G}, \tag{11}$$

where X represents the vapour content in the gas and $p_W^s(T)$ represents the saturation partial pressure given by Magnus' formula:

$$p_W^s(T) = p_m \cdot e^{\frac{C_1 \cdot T}{C_2 + T}}. \quad (12)$$

The parameters p_m, C_1 and C_2 for Eq. (12) are taken from Ref. [40].

The dynamics of the actuators are included in the model as first order lag elements with time constants τ_{1-4}. These additional differential equations are given by

$$\tau_i \frac{d}{dt}\xi_i = (\xi_i - u_i), \quad i = 1, \ldots, 4 \quad (13)$$

with

$$\xi = \left[\dot{m}_{G,\ in}, T_{G,\ in}, \dot{m}_{S,\ in}, A_{Nozzle}\right]^T, \quad (14)$$

$$u = \left[\dot{m}_{G,\ u}, T_u, \dot{m}_{S,\ u}, A_u\right]^T, \quad (15)$$

where A_{Nozzle} represents the nozzle opening of the backpressure valve and u represent the control variables for the *Gas* block, *Heater* block, *Steam* block and backpressure valve shown in Fig. 6. The so obtained coupled set of differential equations (Eqs. (7), (9) and (13)) and coupled output equations for temperature, pressure, relative humidity and mass flow represent the fact that the physical quantities at the testbed are coupled.

Implementation on testbed

The model derived in Section "Dynamic model of hardware setup" is independent of the realised hardware concepts discussed in Section "Hardware concept". By changing one subcomponent (e.g. heater) or implementing a different subconcept (e.g. concept B_F instead of concept A_F) the nonlinear control concept can easily be adapted by adjusting the corresponding time constant τ in Eq. (13).

To implement the derived control concept on the current test setup, the control variables given by Eq. (15) have to be mapped to the actuator signals available at the testbed. This is done by a combination of cascade controllers and characteristic maps obtained from measurements of the realised concepts discussed in Section "Hardware concept".

To obtain the inflowing gas mass stream (*Gas* block, Fig. 6), the orifice plate (concept A_F, Fig. 2a) has been modelled by the nonlinear flow equation given in Eq. (1). The opening area A of the orifice plate has been obtained by performing stationary measurements and applying an offline optimisation. The result is shown in Fig. 7. The different colours show the different pressure set points of the stationary measurements, and the dashed lines show the nonlinear flow equation with the optimised area A. By inverting the nonlinear flow equation (Eq. (1)), the pressure signal for the pressure regulator can be calculated as a function of the desired massflow and the measured backpressure.

The steam (Fig. 4) and backpressure valves (concept B_P, Fig. 5b) are modelled similarly by Eq. (1), but by changing the valve stroke the opening area A of the valves will change. To obtain the nonlinear opening area of the steam and backpressure valves as function of the valve strokes, similar measurements, as for the orifice plate, have to be performed

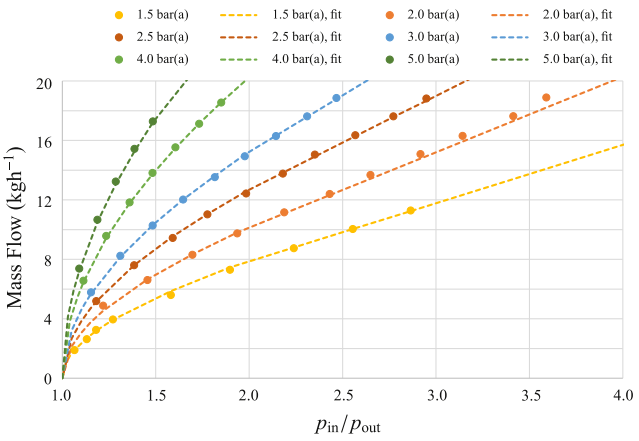

Fig. 7 – Parameterisation of nonlinear flow equation with measurements of the aperture. Plot shows measured data points and the (best) fit result.

for different valve stroke positions. To perform these measurements the valve stroke is increased in 5% increments and the stationary flow is measured. An offline optimisation calculates the opening area for this valve stroke. To obtain the opening area as a function of the valve stroke the points are linearly interpolated. For the steam valve this characteristic map can further be used to calculate the valve stroke as function of the desired massflow and measured pressure drop across the valve. For the backpressure valve the nonlinear opening area is directly used in the model derived in Section "Dynamic model of hardware setup".

As described in Section "Heating", the heating (*Heater* block, Fig. 6) of the inflowing gas is implemented with a heating element and a bypass path (concept C_H, Fig. 3c). The heater is controlled with a cascade controller. This has the advantage that this component can easily be exchanged without the need to remodel and recalculate the nonlinear multivariate controller. The heater characteristic is shown in Fig. 8. This figure has been obtained from stationary measurements. The plot shows measurements for opening and for

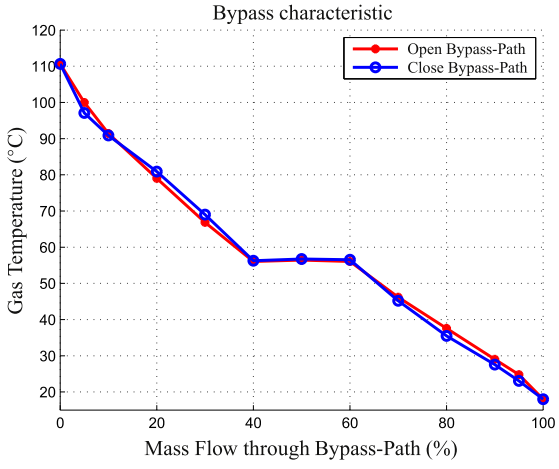

Fig. 8 – Characteristics of the *Heater* (concept C_H, Fig. 3c) obtained from stationary measurements. Data points taken for opening and for closing of the bypass.

Table 1 – Model parameters estimated from measurements.

Parameter	Value
Volume	2972.34 cm^3
T_S	106 °C
γ_G	0.003
γ_S	0.01
τ_1	0.08 s
τ_2	2.5 s
τ_3	0.3 s
τ_4	0.3 s

closing of the bypass-path. The hysteresis behaviour is caused by the thermal inertia of the *Heater*. To increase the temperature dynamics of the gas, the flat part in Fig. 8 can be eliminated by adapting the valve control of the valves in Fig. 3c. To further improve the dynamics, the characteristic map of Fig. 8 can be used as a feedforward signal. Since the valves implemented in the *Heater* have no feedback signal, the output temperature is given as reference value for the control signal.

Model parametrisation from measurements

The model equations Eqs. (7), (9)–(11) and (13) need to be parameterised on the testbed to yield a valid system model. This can be done by a combination of physical parameters taken from literature and measuring step responses of the system to various input steps and performing a multivariate optimisation offline. The so obtained parameters are listed in Table 1. The heat capacities $c_{p,G}$ and $c_{p,S}$ are taken from Ref. [41].

An exemplary step response of the system is given in Fig. 9. The plot clearly shows the coupling of the physical quantities in the system.

The control variables are shown in Fig. 9c. It can be seen that the first three control variables are kept constant while the opening of the backpressure valve is varied. The effect of the variation of this single input on the multivariate system is shown in Fig. 9a. Due to the coupling of the system, the variation of one control variable affects all output variables. To achieve both, good trajectory tracking and disturbance rejection, the controller needs to account for these couplings.

The model parameters given in Table 1 enter into the model equations and affect the dynamic behaviour of these differential equations in various ways. E.g. the parameter *Volume* affects the pressure dynamics of the system. For a series of mass flow changes a system with a large volume needs longer to build up the pressure than a system with a small volume. In Fig. 10 a comparison of the obtained parameterised model with measurement data for the system pressure dynamics is shown.

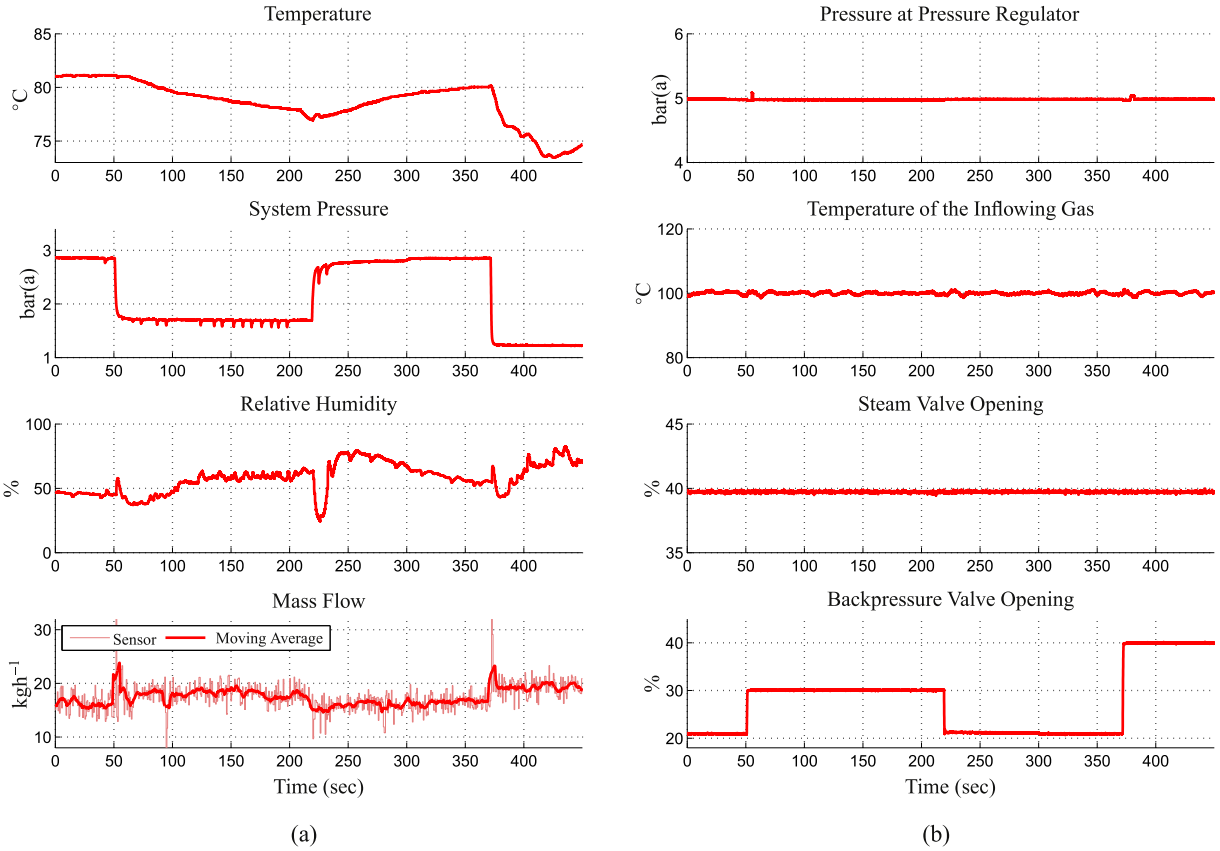

Fig. 9 – The measured step response of the system shows coupling of the system outputs. Plot (a) shows the measured step response of the output *y*, and plot (b) shows the corresponding sensor signals of the control variables *u*. The variation of one input has an effect on all four outputs.

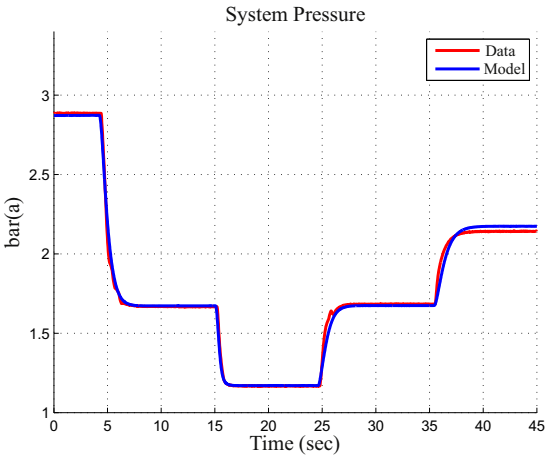

Fig. 10 – Comparison of parameterised model with measurement data.

Nonlinear control design

The model equations Eqs. (7), (9) and (13) are of the structure

$$\begin{aligned} \dot{x} &= f(x) + \sum_{i=1}^{4} g_i(x)u_i, \\ y_j &= h_j(x), \quad j = 1, \ldots, 4 \end{aligned} \tag{16}$$

where the state vector x, input vector u and output vector y are given by

$$x = \begin{bmatrix} m_G \\ m_S \\ T \\ \xi \end{bmatrix}, \quad u = \begin{bmatrix} \dot{m}_{G,\,u} \\ T_u \\ \dot{m}_{S,\,u} \\ A_u \end{bmatrix}, \quad y = \begin{bmatrix} T \\ p \\ \varphi \\ \dot{m}_{out} \end{bmatrix}. \tag{17}$$

For nonlinear systems, which have the form of Eq. (16), the method of exact input-output linearisation [42,43] can be applied. This method uses the so-called *Lie* derivatives to define a nonlinear transformation, which transforms the coupled nonlinear multivariate system into a set of decoupled linear systems. Due to the linearity of the resulting systems linear control methods can be applied.

To obtain a relation between the inputs u and the outputs y, the output functions are derived with respect to time:

$$\begin{aligned} \dot{y}_j &= \frac{\partial h_j}{\partial x}\frac{dx}{dt} = \frac{\partial h_j}{\partial x}\left(f(x) + \sum_{i=1}^{4} g_i(x)u_i\right) \\ &= L_f h_j(x) + \sum_{i=1}^{4} L_{g_i} h_j(x) u_i, \end{aligned} \tag{18}$$

where L_f and L_g represent the *Lie* derivatives of the scalar output function $h(x)$ with respect to $f(x)$ and $g(x)$. If $L_{g_i} h_j(x) = 0, \ \forall i$, then the time derivative $\dot{y}_j$ is independent of u. In that case the time derivative is applied again to the output function. Assuming that δ_j is the smallest integer for which at least one input appears, then $y_j^{(\delta_j)}$ is given by

$$y_j^{(\delta_j)} = L_f^{\delta_j} h_j + \sum_{i=1}^{4} \left(L_{g_i} L_f^{\delta_j - 1} h_j\right) u_i. \tag{19}$$

δ_j is called the *relative degree* of the output y_j. The system Eq. (16) is said to have relative degree of $\Delta = \sum_{j=1}^{4} \delta_j$. Applying this to all outputs of the system one obtains

$$\begin{bmatrix} y_1^{(\delta_1)} \\ y_2^{(\delta_2)} \\ y_3^{(\delta_3)} \\ y_4^{(\delta_4)} \end{bmatrix} = \begin{bmatrix} \ddot{y}_1 \\ \ddot{y}_2 \\ \ddot{y}_3 \\ \dot{y}_4 \end{bmatrix} = \underbrace{\begin{bmatrix} L_f^2 h_1(x) \\ L_f^2 h_2(x) \\ L_f^2 h_3(x) \\ L_f h_4(x) \end{bmatrix}}_{l(x)} + J(x) \begin{bmatrix} u_1 \\ u_2 \\ u_3 \\ u_4 \end{bmatrix}, \tag{20}$$

where $J(x)$ is the so-called decoupling matrix and is required to be regular for control. The elements of the matrix are given by

$$\begin{aligned} J_{i,k}(x) &= L_{g_k} L_f h_i(x), \quad i = 1, 2, 3, \\ J_{4,k}(x) &= L_{g_k} h_4(x), \quad k = 1, \ldots, 4. \end{aligned} \tag{21}$$

As a result of the dimension of the state vector x ($dim(x) = n = 7$), the *relative degree* of the outputs ($\delta_{1,2,3} = 2$, $\delta_4 = 1$) and the complex couplings in the output functions the resulting expression in Eq. (20) are large and are not insightful. For the reason of readability, the detailed calculations of the *Lie* derivatives are not given.

Since $\sum_{j=1}^{4} \delta_j = dim(x) = n$ holds for the system given in Eq. (16) the system has so-called *full relative degree*. For such systems the nonlinear transformation $T(x)$, which transforms it into a linear decoupled system, is given by

$$z = T(x) = \begin{bmatrix} h_1(x) \\ L_f h_1(x) \\ h_2(x) \\ L_f h_2(x) \\ h_3(x) \\ L_f h_3(x) \\ h_4(x) \end{bmatrix}. \tag{22}$$

This leads to the new state space representation of the system, which has the form

$$\dot{z} = A_c z + B_c \beta(x)^{-1}(u - \alpha(x)), \tag{23a}$$

$$u = \alpha(x) + \beta(x)\nu, \tag{23b}$$

with $\alpha(x)$ and $\beta(x)$ defined as

$$\alpha(x) = -\beta(x) l(x), \quad \beta(x) = J^{-1}(x). \tag{24}$$

By inserting Eq. (23b) into Eq. (23a) the system transforms into

$$\dot{z} = A_c z + B_c \nu \tag{25}$$

where A_c and B_c are matrices in controllable canonical form [44]. Eq. (25) represents a decoupled linear system with the new *synthetic* input vector ν. For the transformed system linear control methods can be applied. Additionally, the choice of the state feedback control Eq. (23b) transforms Eq. (20) to

$$\begin{bmatrix} y_1^{(\delta_1)} \\ y_2^{(\delta_2)} \\ y_3^{(\delta_3)} \\ y_4^{(\delta_4)} \end{bmatrix} = \begin{bmatrix} \ddot{y}_1 \\ \ddot{y}_2 \\ \ddot{y}_3 \\ \dot{y}_4 \end{bmatrix} = \begin{bmatrix} \nu_1 \\ \nu_2 \\ \nu_3 \\ \nu_4 \end{bmatrix}, \tag{26}$$

which represents an input-output behaviour of the new *synthetic* inputs ν_{1-4} to the outputs y_{1-4} as chain of δ_{1-4} integrators.

For additional control the tracking errors can be defined as

$$e_j = y_j(t) - r_j(t), \quad j = 1, \ldots, 4 \tag{27}$$

where $r_j(t)$ is a reference trajectory, which the system output $y_j(t)$ should follow. The tracking error vector can be expanded by the additional terms

$$e_{j,0} = \int_0^t e_j(\tau)d\tau, \quad e_{j,1} = e_j, \quad e_{j,2} = \dot{e}_j, \tag{28}$$

which can be used to design a Two-Degree-of-Freedom (2DoF) controller. The new *synthetic* input ν can be written as a combination of a feedforward part, which exploits Eq. (26), and a PID controller:

$$\begin{aligned} \nu_k &= \ddot{r}_k - K_{I,k}\, e_{k,0} - K_{P,k}\, e_{k,1} - K_{D,k}\, e_{k,2}, \quad k = 1,2,3 \\ \nu_4 &= \dot{r}_4 - K_{I,4}\, e_{4,0} - K_{P,4}\, e_{4,1} - K_{D,4}\, e_{4,2}, \end{aligned} \tag{29}$$

where $\ddot{r}$ and $\dot{r}$ represent the time derivatives of the reference trajectory and $K_{P,1-4}$, $K_{I,1-4}$ and $K_{D,1-4}$ are the gains of the four PID controllers.

The resulting 2DoF controller is shown in Fig. 11. The Σ^{-1} block represents Eq. (23b) and performs the decoupling of the system. The decoupling is a nonlinear function of the state vector x and, therefore, requires the current states. In the presented model, the property of *differential flatness* [45,46] of the system can be used to calculate the state vector x from the reference trajectories r offline and use it as input for the decoupling block Σ^{-1}.

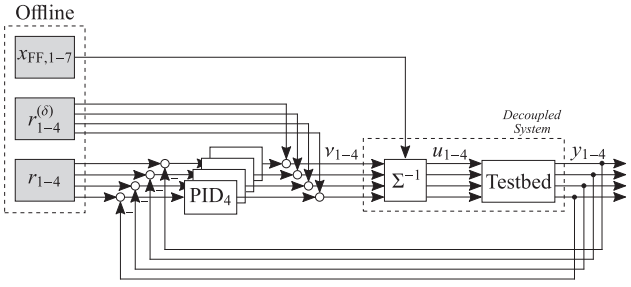

Fig. 11 – Block diagram of the Two-Degree-of-Freedom (2DoF) controller. To each decoupled linear system a PID controller is applied.

Together with the testbed the Σ^{-1} block forms four decoupled linear systems. Each of these linear systems has a feedforward control and a feedback controller given by Eq. (29).

Observer design

The used coriolis sensor for the mass flow measurement shows a measurement inaccuracy in the measurement range and has additionally a measurement lag, which makes it not suitable for transient measurements. Therefore, a *Luenberger* Observer [47] for the mass flow, based on the dynamics of the decoupled system given by Eq. (25), was designed for control. For mass flow transients the observer gain is set to zero, which prevents the observer from being affected by the measurement lag. This proved to achieve good results for control. An alternative approach would be using just the feedforward control during mass flow transitions.

Table 2 – Hardware components used for setup.

Component	Hardware type	Specifications
Fig. 2a, PC	Pressure regulator	$T_{90} < 0.1$ s
Fig. 2a, OP	Orifice plate	Ø 2.5 mm
Fig. 3c, CV_1	Seat valve	C_{vs} 0.92
Fig. 3c, CV_2	Seat valve	C_{vs} 1.39
Fig. 3c, HEX	Heat exchanger	800 W
Fig. 4, D_1	Saturated steam boiler	42.5 kg h^{-1} at 6 bar(a)
Fig. 4, CV	Sliding gate valve	C_{vs} 1.27
Fig. 5b, CV	Sliding gate valve	C_{vs} 9.24

Results and measurements

Experimental studies were conducted in order to validate the hardware concept, the thermodynamic model and the implemented nonlinear multivariate control concept.

The selected hardware components used for the test bed are listed in Table 2. The coriolis sensor used to measure the mass flow has been chosen such that the pressure drop is minimal and, therefore, the accuracy at lower mass flow ranges is limit. Hence the observer, as introduced in Section "Observer Design", has been used as reference signal for the controller.

Mechatronic setup

A schematic of the experimental control setup is shown in Fig. 12. The control algorithm is implemented in Matlab/Simulink and uploaded to a dSpace MicroAutoBox II 1511/1512, where it runs in a real-time environment. The depicted programmable logic controller (PLC) is mainly used for signal conversion and to provide basic safety measures. The fuel cell stack is represented by an applied measuring section. It includes sensors for pressure p, air temperature T, humidity φ and mass flow $\dot{m}$. The application of a real fuel cell stack would introduce an additional pressure resistance, which is in series with the back pressure valve, and would act as a disturbance on the control.

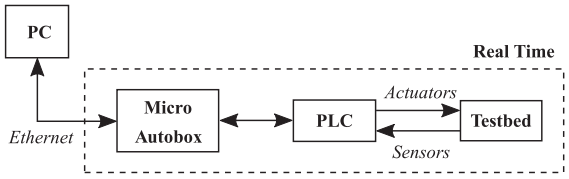

Fig. 12 – Schematic of control setup on testbed.

The used parameter configuration of the four 2DoF controllers are shown in Table 3.

Table 3 – 2DoF control parameters for measurement.

Output	K_P	K_I	K_D
T	2	0.001	15
p	6	3	0
φ	5	1	5
$\dot{m}_{out}$	1	0.1	0

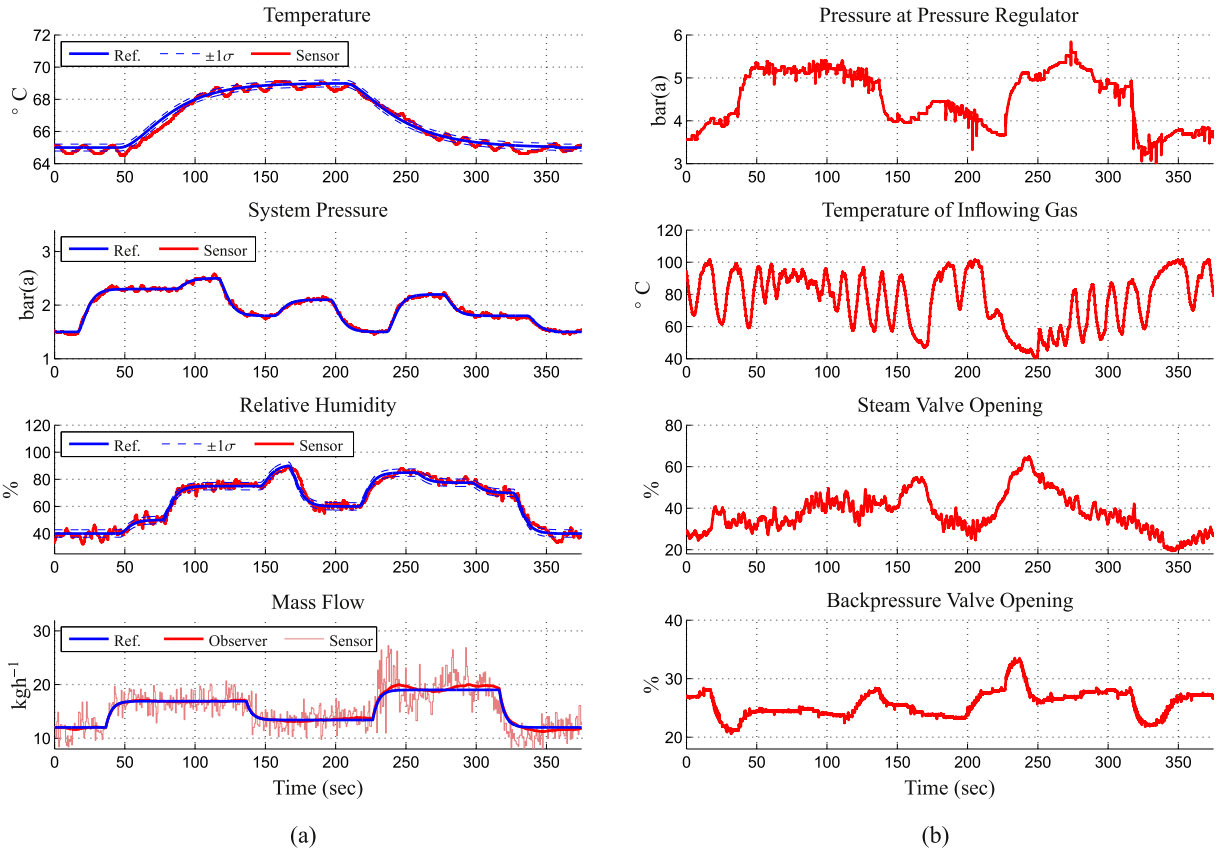

Fig. 13 – Plot (a) shows the decoupled system following the reference trajectories. Plot (b) shows the corresponding sensor signals of the control variables.

Experimental results

For validation of the controller, four different random reference trajectories $r(t)$ have been generated and loaded onto the system. The results are shown in Fig. 13. Fig. 13a displays the reference trajectories in blue and the measured sensor signals in red. The standard deviation is indicated in dashed blue lines. As discussed in Section "Observer Design", the 2DoF control of the mass flow is based on an observer. In the bottom plot in Fig. 13a, both measurement and observer signals are shown.

In Fig. 13a it can be seen that the controller successfully decouples the system and the outputs y can independently follow their desired reference trajectories.

The resulting control variables u are shown in Fig. 13b. Due to the high thermal inertia of the system, the 2DoF control for the gas temperature has been parameterised such that the time constant is very small, and therefore it behaves almost like a two-point controller. This leads to the control performance shown in the second plot in Fig. 13b. The control input variation is very fast, but the output functions given in Fig. 13a show a good performance.

The numeric values of the standard deviations obtained from stationary and dynamic measurements are presented in Table 4. The first column shows the measurement results for the reference trajectories if they are kept constant. The second column shows the measurement results for dynamic operation. The values for dynamic operation are calculated based on the measurement given in Fig. 13.

Table 4 – Standard deviations for stationary and dynamic measurements.

Output	σ_{stat}	σ_{dyn}
T	0.16 °C	0.21 °C
p	0.03 bar(a)	0.03 bar(a)
φ	2.60%	2.75%
$\dot{m}_{out}$ (Obs.)	0.17 kg h^{-1}	0.50 kg h^{-1}
$\dot{m}_{out}$ (Sens.)	1.79 kg h^{-1}	2.20 kg h^{-1}

Conclusion

This paper presents a novel approach for a dynamic testbed for PEMFC stack testing. Different approaches have been evaluated to provide the stack with an inflowing gas mass flow, gas temperature, relative humidity of the inflowing gas and stack pressure. Based on the evaluation, a test setup was constructed and a nonlinear multivariate model, based on the hardware setup, was derived. In order to achieve a better dynamic response, the actuator dynamics were incorporated as first order lag elements. To yield a valid system description, the derived model has been parameterised with measurements performed at the testbed.

Due to the coupling of the thermodynamic quantities in the system and the nonlinearity of the model, a nonlinear

multivariate controller has been designed, which is based on the method of exact input-output linearisation. This leads to a decoupling of the system and allows for the implementation of a 2DoF controller, which has feedback and feedforward control for each of the system outputs.

The performance of the realised hardware concept was demonstrated, and it showed that the applied nonlinear control concept ensures trajectory tracking during dynamic set point changes. The presented measurement results validate the control performance.

Acknowledgement

This work was accomplished in the course of the funded project FCH Media in collaboration of HyCentA Research GmbH, AVL List GmbH and TU Wien. The authors would like to thank the Austrian Ministry of Innovation and Technology (BMVIT, Mobilität der Zukunft programme) for financially supporting this research project.

REFERENCES

[1] Core Writing Team. In: Pachauri RK, Meyer LA, editors. IPCC, 2014: climate change 2014: synthesis report. Contribution of working groups I, II and III to the fifth assessment report of the intergovernmental panel on climate change. Geneva, Switzerland: Tech. rep., IPCC; 2014.
[2] Eichlseder H, Klell M. Wasserstoff in der Fahrzeugtechnik: Erzeugung. 3rd ed. Speicherung, Anwendung: Springer Vieweg; 2012.
[3] U.S. Department of Energy. Annual Progress Report, Tech. Rep. DOE/GO-102015-104731, DOE Hydrogen and Fuel Cells Program (2015). 2015.
[4] Pollet BG, Staffell I, Shang JL. Current status of hybrid, battery and fuel cell electric vehicles: from electrochemistry to market prospects. Electrochim Acta 2012;84:235–49. https://doi.org/10.1016/j.electacta.2012.03.172.
[5] Yoshida T, Kojima K. Toyota MIRAI fuel cell vehicle and progress toward a future hydrogen society. Electrochem Soc Interface 2015;24(2):45–9. https://doi.org/10.1149/2.F03152if.
[6] Sung W, Song Y-I, Yu K-H, Lim T-W. Recent advances in the development of Hyundai Kia's fuel cell electric vehicles. SAE Int J Engines 2010;3:768–72. https://doi.org/10.4271/2010-01-1089.
[7] Yamaguchi N, Iwai A, Fukushima T, Shinoki H. New drive motor for fuel cell vehicle FCX clarity. 2009. https://doi.org/10.4271/2009-01-1001. URL http://papers.sae.org/2009-01-1001/.
[8] Kreuer K-D, editor. Fuel cells. New York: Springer; 2013. https://doi.org/10.1007/978-1-4614-5785-5.
[9] Brandstätter S, Striednig M, Aldrian D, Trattner A, Klell M. Highly integrated fuel cell analysis infrastructure for advanced research topics, SAE Technical Paper 2017-01-1180. 2017. https://doi.org/10.4271/2017-01-1180.
[10] Wang Y, Wang C-Y. Transient analysis of polymer electrolyte fuel cells. Electrochim Acta 2005;50(6):1307–15. https://doi.org/10.1016/j.electacta.2004.08.022.
[11] Wang Y, Wang C-Y. Dynamics of polymer electrolyte fuel cells undergoing load changes. Electrochim Acta 2006;51(19):3924–33. https://doi.org/10.1016/j.electacta.2005.11.005.
[12] Kang S, Min K, Yu S. Two dimensional dynamic modeling of a shell-and-tube water-to-gas membrane humidifier for proton exchange membrane fuel cell. Int J Hydrogen Energy 2010;35(4):1727–41. https://doi.org/10.1016/j.ijhydene.2009.11.105.
[13] Kang S, Min K, Yu S. Dynamic modeling of a proton exchange membrane fuel cell system with a shell-and-tube gas-to-gas membrane humidifier. Int J Hydrogen Energy 2012;37(7):5866–75. https://doi.org/10.1016/j.ijhydene.2011.12.063.
[14] Hao L, Yu H, Hou J, Song W, Shao Z, Yi B. Transient behavior of water generation in a proton exchange membrane fuel cell. J Power Sources 2008;177(2):404–11. https://doi.org/10.1016/j.jpowsour.2007.11.034.
[15] Migliardini F, Unich A, Corbo P. Experimental comparison between external and internal humidification in proton exchange membrane fuel cells for road vehicles. Int J Hydrogen Energy 2015;40(17):5916–27. https://doi.org/10.1016/j.ijhydene.2015.03.012.
[16] Jiao K, Alaefour IE, Karimi G, Li X. Cold start characteristics of proton exchange membrane fuel cells. Int J Hydrogen Energy 2011;36(18):11832–45. https://doi.org/10.1016/j.ijhydene.2011.05.101.
[17] Jiao K, Alaefour IE, Karimi G, Li X. Simultaneous measurement of current and temperature distributions in a proton exchange membrane fuel cell during cold start processes. Electrochim Acta 2011;56(8):2967–82. https://doi.org/10.1016/j.electacta.2011.01.019.
[18] Kong IM, Jung A, Kim BJ, Baik KD, Kim MS. Experimental study on the start-up with dry gases from normal cell temperatures in self-humidified proton exchange membrane fuel cells. Energy 2015;93(Part 1):57–66. https://doi.org/10.1016/j.energy.2015.09.014.
[19] Zhang Q, Lin R, Tcher L, Cui X. Experimental study of variable operating parameters effects on overall PEMFC performance and spatial performance distribution. Energy 2016;115(Part 1):550–60. https://doi.org/10.1016/j.energy.2016.08.086.
[20] Santarelli M, Torchio M. Experimental analysis of the effects of the operating variables on the performance of a single PEMFC. Energy Convers Manag 2007;48(1):40–51. https://doi.org/10.1016/j.enconman.2006.05.013.
[21] Santarelli M, Torchio M, Cal M, Giaretto V. Experimental analysis of cathode flow stoichiometry on the electrical performance of a PEMFC stack. Int J Hydrogen Energy 2007;32(6):710–6. https://doi.org/10.1016/j.ijhydene.2006.08.008.
[22] Corbo P, Migliardini F, Veneri O. Performance investigation of 2.4 kW PEM fuel cell stack in vehicles. Int J Hydrogen Energy 2007;32(17):4340–9. https://doi.org/10.1016/j.ijhydene.2007.05.043.
[23] Hamelin J, Agbossou K, Laperrire A, Laurencelle F, Bose T. Dynamic behavior of a PEM fuel cell stack for stationary applications. Int J Hydrogen Energy 2001;26(6):625–9. https://doi.org/10.1016/S0360-3199(00)00121-X.
[24] Yan Q, Toghiani H, Causey H. Steady state and dynamic performance of proton exchange membrane fuel cells (pemfcs) under various operating conditions and load changes. J Power Sources 2006;161(1):492–502. https://doi.org/10.1016/j.jpowsour.2006.03.077.
[25] Park S-K, Choe S-Y, Ho Choi S. Dynamic modeling and analysis of a shell-and-tube type gas-to-gas membrane humidifier for PEM fuel cell applications. Int J Hydrogen Energy 2008;33(9):2273–82. https://doi.org/10.1016/j.ijhydene.2008.02.058.
[26] Park S-K, Choe S-Y, Lim T-W, Kim J-S, Seo D-H, Choi J. Analysis of a shell-and-tube type gas-to-gas membrane humidifier for an automotive polymer electrolyte membrane fuel cell power system. Int J Automot Technol 2013;14(3):449–57. https://doi.org/10.1007/s12239-013-0049-4.

[27] Tang Y, Yuan W, Pan M, Li Z, Chen G, Li Y. Experimental investigation of dynamic performance and transient responses of a kw-class PEM fuel cell stack under various load changes. Appl Energy 2010;87(4):1410–7. https://doi.org/10.1016/j.apenergy.2009.08.047.
[28] Kim B, Cha D, Kim Y. The effects of air stoichiometry and air excess ratio on the transient response of a PEMFC under load change conditions. Appl Energy 2015;138:143–9. https://doi.org/10.1016/j.apenergy.2014.10.046.
[29] Kancsár J, Kozek M, Jakubek S. Flatness-based feedforward control of polymer electrolyte membrane fuel cell gas conditioning system. Int J Hydrogen Energy 2016;41(39):17526–38. https://doi.org/10.1016/j.ijhydene.2016.06.086.
[30] Danzer MA, Wilhelm J, Aschemann H, Hofer EP. Model-based control of cathode pressure and oxygen excess ratio of a PEM fuel cell system. J Power Sources 2008;176(2):515–22. https://doi.org/10.1016/j.jpowsour.2007.08.049.
[31] Danzer MA, Wittmann SJ, Hofer EP. Prevention of fuel cell starvation by model predictive control of pressure, excess ratio, and current. J Power Sources 2009;190(1):86–91. https://doi.org/10.1016/j.jpowsour.2008.12.089.
[32] Hähnel C, Aul V, Horn J. Power control for efficient operation of a pem fuel cell system by nonlinear model predictive control. IFAC-PapersOnLine 2015;48(11):174–9. https://doi.org/10.1016/j.ifacol.2015.09.179.
[33] Fang C, Xu L, Cheng S, Li J, Jiang H, Ouyang M. Sliding-mode-based temperature regulation of a proton exchange membrane fuel cell test bench. Int J Hydrogen Energy 2017;42(16):11745–57.
[34] Patterson TW, Darling RM. Damage to the cathode catalyst of a pem fuel cell caused by localized fuel starvation. Electrochem Solid-State Lett 2006;9(4):A183–5.
[35] Gu W, Paul TY, Carter RN, Makharia R, Gasteiger HA. Modeling of membrane-electrode-assembly degradation in proton-exchange-membrane fuel cells–local H2 starvation and start–stop induced carbon-support corrosion. In: Modeling and diagnostics of polymer electrolyte fuel cells. Springer; 2009. p. 45–87.
[36] Venturi M, Sang J, Knoop A, Hornburg G. Air supply system for automotive fuel cell application, SAE Technical Paper. 2012.
[37] Lehmann J, Luschtinetz T. Wasserstoff und Brennstoffzellen: Unterwegs mit dem saubersten Kraftstoff. Springer-Verlag; 2014.
[38] Zawodzinski TA, Derouin C, Radzinski S, Sherman RJ, Smith VT, Springer TE, et al. Water uptake by and transport through Nafion 117 membranes. J Electrochem Soc 1993;140(4):1041–7.
[39] Chorin AJ, Marsden J. A mathematical introduction to fluid mechanics. 3rd ed. New York: Springer-Verlag; 1993.
[40] Plant RS, Yano J-I. In: Parameterization of atmospheric convection, vol. 1. Imperial College Press; 2015.
[41] VDI-Gesellschaft Verfahrenstechnik und Chemieingenieurwesen. VDI Wärmeatlas. Berlin, Heidelberg: Springer Berlin Heidelberg; 2013.
[42] Slotine J-J, Li W. Applied nonlinear control. Prentice Hall; 1991.
[43] Khalil HK. In: Nonlinear systems, vol. 3. Prentice Hall; 2002.
[44] Isidori A. Nonlinear control systems. 3rd ed. Secaucus, NJ, USA: Springer-Verlag New York, Inc.; 1995.
[45] Fliess M, Lévine J, Martin P, Rouchon P. Flatness and defect of non-linear systems: introductory theory and examples. Int J Control 1995;61(6):1327–61. https://doi.org/10.1080/00207179508921959.
[46] Fliess M, Lévine J, Martin P, Rouchon P. A lie-backlund approach to equivalence and flatness of nonlinear systems. IEEE Trans Automatic Control 1999;44(5):922–37. https://doi.org/10.1109/9.763209.
[47] Luenberger DG. Observing the state of a linear system. IEEE Trans Mil Electron 1964;8(2):74–80.